Springer

KSME

Journal of Mechanical Science and Technology 33 (5) (2019) 2429~2438
www.springerlink.com/content/1738-494x(Print)/1976-3824(Online)
DOI 10.1007/s12206-019-0242-0

Effects of expansion pipe length on heat transfer enhancement of impinging jet array †

Kirttayoth Yeranee[1], Makatar Wae-hayee[1,*], Ibroheng Piya[2], Yu Rao[3] and Chayut Nuntadusit[1]

[1]*Department of Mechanical Engineering, Faculty of Engineering, Prince of Songkla University, Hat Yai, Songkhla, 90112, Thailand*
[2]*Department of Mechanical Engineering, Faculty of Engineering, Princess of Naradhiwas University, Narathiwat, 96000, Thailand*
[3]*School of Mechanical Engineering, Shanghai Jiao Tong University, Shanghai, 200240, China*

(Manuscript Received April 19, 2018; Revised October 24, 2018; Accepted November 2, 2018)

Abstract

We experimentally and numerically investigated the effect of expansion pipe length on heat transfer enhancement and flow characteristics of impinging jet array with mounting expansion pipe. The inner diameter (d) and the length of each main pipe nozzle was d = 17.2 mm and 200 mm, respectively. Nozzle arrangement was distributed in 5 rows × 5 columns with an in-line configuration. The jet-to-wall distance (H) was fixed at H/d = 8, while the jet-to-jet spacing (S) was varied at S/d = 6 and 8. The expansion pipe length (L) was varied at L/d = 4, 6 and 8, and the inner diameter of the expansion pipe (D) was fixed at D/d = 4. Reynolds number of the jets was kept constant at 30000. The conventional impinging jets were also performed to compare with the case of jets with mounting expansion pipe. The 3-D numerical simulation with v^2-f turbulence model was applied to simulate the flow characteristics. Results showed that the surrounding air was induced into the expansion pipe, and an entrainment of induced air became greater when expansion pipe was longer. This influenced more markedly on enhancement of Nusselt number at stagnation point for narrow jet-to-jet spacing (S/d = 6).

Keywords: Heat transfer enhancement; Multiple impinging jets; Expansion pipe; CFD

1. Introduction

Jet impingement is applied in thermal engineering industrial processes, such as in the annealing of glass or metal, the drying of textiles or paper, and the cooling of gas turbine vanes or electronic devices, due to its high heat transfer at stagnation regions. Basically, maximum heat transfer at the stagnation point of a single impinging jet is discovered at the end of the potential core. This is found generally in the range of four- and six-times of nozzle diameter from jet outlet [1-3].

In the case of impinging jet arrays, two important affecting factors in impinging flow and heat transfer characteristics on the target surface are jet interference with adjacent jets before impinging on the surface, and jet fountain on the wall after impingement. Jet interference with adjacent jets is particularly strong when the jet-to-wall distance is higher and the jet-to-jet spacing is narrower. This is in contrast to the jet fountain from the collision of wall jets, in that it is particularly stronger when the jet-to-wall distance becomes shorter and the jet-to-jet spacing is larger [3-6].

Heat transfer rate of impinging jets is governed by two principal factors: momentum of jet impinging on the wall, and turbulent intensity of jet before impinging. Increasing of momentum of jet requires the power of pump or fan, while the method to increase turbulent intensity could be classified according to external power requirement into two methods: Active and passive. Active method is using external power to activate fluid flow, while passive method requires no external source. Passive methods are thus adopted by many researchers to achieve high heat transfer in impinging jets.

Increasing turbulent intensity of jet flows to enhance heat transfer on the impingement surface could be found in many studies such as adding of triangular tabs [7, 8] or mesh screen [9, 10] to the nozzle exits; inserting twisted tape [11-14] or guide vanes [15, 16] into the nozzle; or modifying the nozzle geometry [17, 18]. Expanding jet outlet is one of the methods to enhance turbulent intensity before impingement, since this would increase entrainment of ambient fluid into the jet flow [19, 20]. Therefore, increasing entrainment of ambient fluid into jet flow is an important factor to enhance turbulent intensity. Generally, this method is applied in combustion of industrial applications for enhancing the mixing and spreading of flame jets [21]. However, it is rarely adopted for enhancement of heat transfer on impingement region.

In Yeranee et al. [22], one of our previous studies, an array of impinging jet mounting an expansion pipe to enhance heat

*Corresponding author. Tel.: +66 7428 7231, Fax.: +66 7455 8830
E-mail address: wmakatar@eng.psu.ac.th
† Recommended by Associate Editor Ji Hwan Jeong

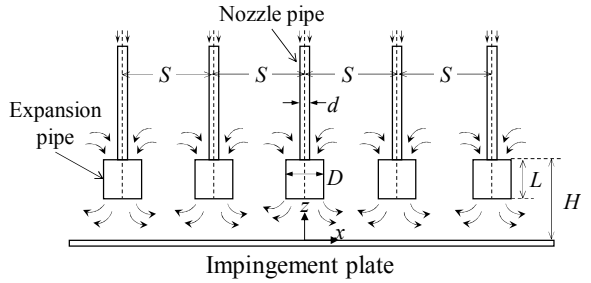

(a) Impinging jets from pipe nozzles with expansion pipes

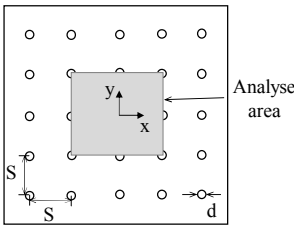

(b) Inlined 5 × 5 nozzle arrangement

Fig. 1. Experimental model of impinging jet array.

transfer on impingement surface was investigated. Results showed that the case of mounting expansion pipe could induce ambient air into the jet flow more than the case of conventional jet, and hence heat transfer on the impingement surface is higher. Acceleration of the surrounding air into the expansion pipe was from the suction force resulting from the low pressure inside the expansion pipe due to kinetic effect. Suction force was envisioned to be dependent on the expansion pipe length since varying pressure should result from different length. Therefore, the effect of expansion pipe length on the heat transfer and flow characteristics of impinging jet array is attractive to be further studied.

The aim of this study was to investigate the effect of expansion pipe length on heat transfer enhancement and flow characteristics, experimentally and numerically. Moreover, jet-to-jet spacing (S/d) was examined to seek a condition having a high heat transfer rate on the impingement surface. Conventional jets (without expansion pipes) were also examined for comparing with the case of mounting expansion pipes based on the same jet Reynolds number.

2. Experimental apparatus and method

2.1 Model and parameters

The experimental model of impinging jets with mounting expansion pipe is shown in Fig. 1. Jets discharging from the pipe nozzles impinged perpendicularly on the wall. Expansion pipes were mounted at the end of each pipe nozzle with the same centerlines. Nozzle arrangement was 5 rows × 5 columns with in-line configuration. An origin of the Cartesian coordinates was assigned on the impingement wall with the same location of middle jet centerline. The X-axis and the Y-axis were on the orthogonal plane normal to the jet, and the Z-axis was along the axial of the jet.

Table 1. Detail of experimental parameters.

Inner diameter of main pipe nozzle (d)	d = 17.2 mm
Length of expansion pipe (L)	L/d = 4, 6, 8
Inner diameter of expansion pipe (D)	D/d = 4
Jet-to-wall distance (H)	H/d = 8
Jet-to-jet spacing (S)	S/d = 6, 8
Reynolds number (Re)	Re = 30000

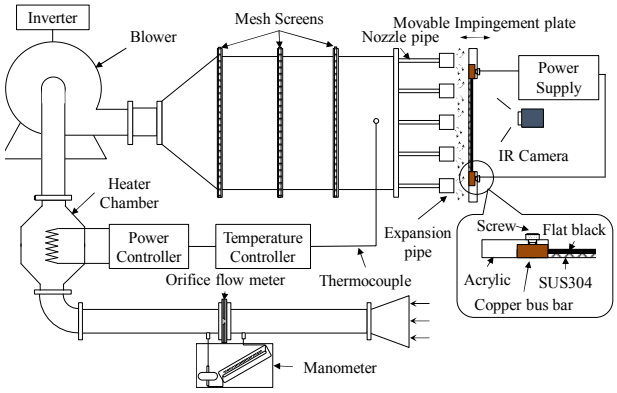

Fig. 2. Diagram of the experimental apparatus.

The inner diameter and the length of main pipe nozzle was d = 17.2 mm and 200 mm, respectively. The inner diameter of the expansion pipe (D) was fixed at four-times of d (D/d = 4), due to this condition getting high heat transfer in the preliminary study of single impinging jet [23]. The lengths (L) of expansion pipe were varied at L/d = 4, 6 and 8. The jet-to-wall distance (H) was fixed at H/d = 8, and the jet-to-jet spacing (S) was varied at S/d = 6 and 8. The jet Reynolds number based on the nozzle diameter and the average jet velocity was kept constant at 30000. Details of the experimental parameters are summarized in Table 1.

2.2 Experimental apparatus

A diagram of the experimental setup is given in Fig. 2. The air is accelerated by the centrifugal blower and passes through the orifice flow-meter. Subsequently, the air enters the temperature controlled chamber equipped with a 12-kW heater to control the jet outlet temperature at 27 °C. The flow rate of the air jet is assigned according to required Reynolds number. The jet chamber is mounted with three perpendicular separate layers of mesh plates to ensure a uniform flow field approaching the pipe nozzles and a uniform jet temperature at the pipe exit. The jet issuing from the pipe nozzle with a length of 200 mm impinges upon the target surface. The pipe is designed such that it is sufficiently long to ensure a fully developed flow at the pipe exit. The impingement plate is movable in the Z-axis to adjust for the required jet-to-wall distance.

Expansion pipes made of 0.5-mm stainless sheet were rolled to form a cylindrical shape. The expansion pipes were

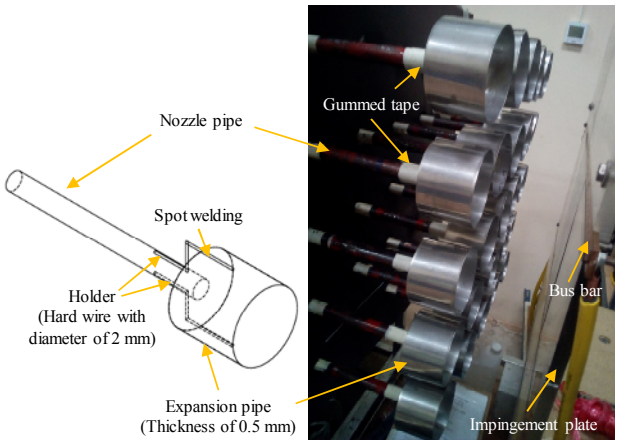

Fig. 3. The details of pipe nozzle and expansion pipe connection.

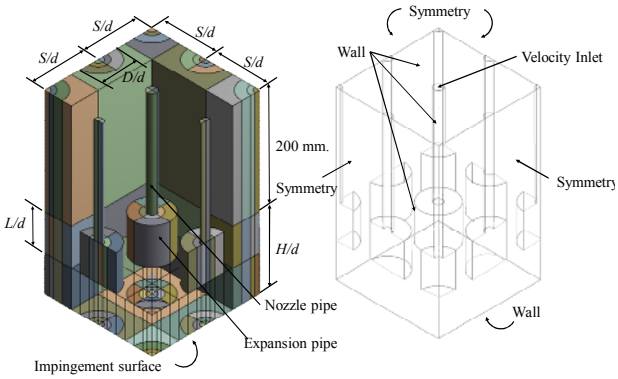

Fig. 4. Numerical model and boundary conditions.

connected to a pair of hard wires having diameter of 2 mm by spot welding and were assembled to the pipe nozzles as shown in Fig. 3. The centerlines of the expansion pipes and the pipe nozzles were concentric. The nozzle pipe outlet and the expansion pipe inlet were matched in the same position of axial direction.

2.3 Data reduction

The impingement plate was made of a rectangular acrylic plate having 830 × 830 mm^2 in size, 15 mm in thickness and 280 × 280 mm^2 square hollow at its center. A very thin stainless steel sheet (0.03 mm in thickness) was tightly stretched between two copper bus bars over the hollow of the acrylic plate. The slim thickness of the stainless steel sheet was to ensure that temperatures on both sides did not significantly differ [23]. An infrared camera (FLIR, T420) was installed on the opposite side of the impingement surface to measure temperature distributions on the sheet. The camera, with detector of 320 × 240 pixels, was connected to a PC with FLIR tool software. The measured surface was coated with flat black spray having emissivity of 0.95.

DC electrical current was applied to the stainless steel sheet through the copper bus bars. The stainless steel sheet, treated as a constant input heat flux, was cooled by the impinging jets. The input heat flux ($\dot{Q}_{input}$) can be calculated from Eq. (1):

$$\dot{Q}_{input} = VI / A \,, \tag{1}$$

where I is the electrical current; V, the voltage across the bus bars; and A, stainless steel foil area.

The local heat transfer coefficient (h) can then be evaluated from Eq. (2):

$$h = \frac{\dot{Q}_{input} - \dot{Q}_{loss,r} - \dot{Q}_{loss,c}}{T_w - T_{aw}} \,, \tag{2}$$

where $\dot{Q}_{loss,r} = \sigma\varepsilon(T_w^4 - T_s^4)$ and $\dot{Q}_{loss,c} = h_{loss,c}(T_w - T_s)$ are the heat losses from the rear side of the jet impingement wall to surrounding by radiation, and natural convection, respectively; T_w, the local wall temperature; T_{aw}, the local adiabatic wall temperature (during jets impinging without heat flux); σ, the Stefan-Boltzmann constant; ε, the emissive coefficient of the captured side; T_s, the ambient temperature; and $h_{loss,c}$, the heat transfer coefficient calculated from the natural convective heat transfer from the vertical surface to the surrounding.

The local Nusselt number (Nu) is calculated using Eq. (3):

$$Nu = hd / k \,, \tag{3}$$

where d is the nozzle inner diameter; and k, the thermal conductivity of the air jet.

The average Nusselt number on the impingement surface ($\overline{Nu}$) is evaluated using Eq. (4):

$$\overline{Nu} = \bar{h}d / k \,, \tag{4}$$

where $\bar{h}$ is the average heat transfer coefficient calculated from the average wall temperature.

The uncertainty of the Nusselt number was in the range of 3.37 % to 5.28 % using the calculation method suggested by Kline and Mcclintock [24]. This uncertainty range is the same range that was used in previous work studying jet impingement [25, 26].

3. Numerical simulation

3.1 Numerical model and its boundary conditions

For numerical simulation, commercial software ANSYS FLUENT (version 15.0) was employed. The 3-D numerical model, as shown in Fig. 4 together with associated boundary conditions, was created in accordance with the experiment. The model was divided into three sections for clarity. The first section concerns the 200 mm-long main pipe nozzles with diameter (d) of 17.2 mm. The second section involves the expansion pipes attached to the end of the main pipe nozzles. The third section is the impingement region. The uniform velocity assigned at velocity inlet is 27.21 m/s. Details of all

Table 2. Detail of simulation boundary conditions.

Boundary condition	As defined
Velocity inlet	27.21 m/s (*Re* = 30000)
4-side lateral surface	Symmetry
Upper and lower surface	Wall

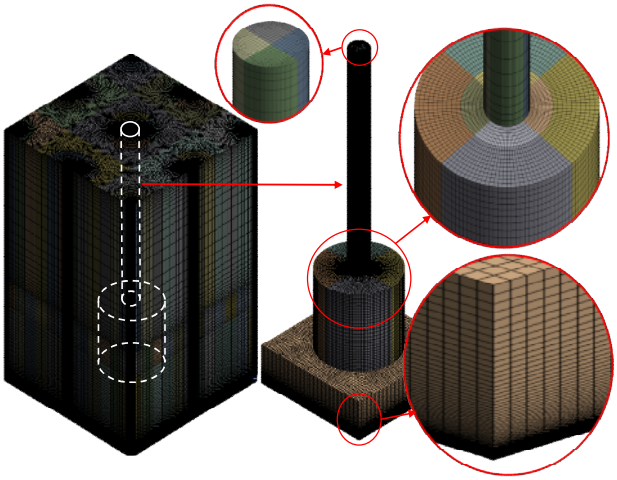

Fig. 5. Grid system for the simulation model.

boundary conditions are summarized in Table 2.

3.2 Grid system

The majority of the shape of the generated grid applied in the domain was rectangular cubic as shown in Fig. 5. The grids were refined in stagnation regions, which the jet has high velocity gradient at near-impingement surface. The dimensionless wall distance (y^+) of the first grid was defined by Eq. (5):

$$y^+ = \frac{y_1 u_\tau}{v}, \tag{5}$$

where y_1 is the distance of the first node to the wall; u_τ, the friction velocity; and v, kinematic viscosity of the air.

Numerical grids were varied to attain a solution with accuracy $y^+ \leq 1$ [27]. At saturation of the variations, the number of grids with 2982080 elements was found, and was adopted in this numerical simulation. Details of numerical accuracy had already been elaborated in our previous work [22].

3.3 Numerical procedures

Reynolds averaged continuity and Navier-Stokes equations accompanying boundary conditions were solved to obtain the resulting flow field. The normal-velocity relaxation model (v^2-f turbulence model) was applied in this simulation due to excellently predicted solutions and moderate computation cost [28]. It has been adopted in many numerical jet impingement problems. Results employing this simulation have been proven to agree very well with experimental results [29]. Pressure-velocity coupling was handled by the SIMPLE algorithm with second-order upwind scheme, and PRESTO algorithm was employed for the pressure spatial discretization [30]. The iterations of the computation were considered to be converged when the residual of continuity and momentum solutions was less than 1×10^{-5} [31, 32].

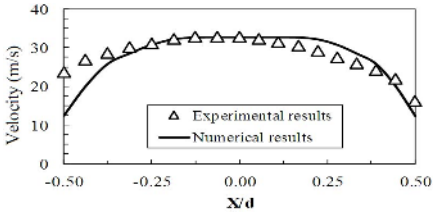

Fig. 6. Velocity profiles at nozzle outlet of central jet (Y/d = 0, Re = 30000).

4. Results and discussion

4.1 Flow characteristics

To validate simulation results, the jet velocity profiles at pipe outlet of central jet from simulation and experimental results were compared as shown in Fig. 6. The numerical results agreed with the experimental data. However, there was a small discrepancy at the edge of the pipe nozzle.

Flow characteristics simulated using CFD for conventional jets and the jets with expansion pipe were compared to understand basically the effect of the mounting expansion pipe at the jet outlets. Velocity-vector field of impinging jets on *Z*-*X* plane at the middle pipe nozzle (*Y*/*d* = 0) at *S*/*d* = 6 is shown in Fig. 7(a) for conventional jets, and in Fig. 7(b) for jets with expansion pipe at *L*/*d* = 4. In the former without expansion pipe, surrounding air was initially induced by jet flow at the nozzle outlets (Circle mark 1), and was continuously entrained during the flow (Circle mark 2). In the latter with expansion pipe, air entrainment at the nozzle outlets (Circle mark 1) and jet flow (Circle mark 2) was at least 1.5-times of those in the former. The increase of surrounding air entering into the expansion pipe can be visualized by the longer vectors in the expansion pipe in comparison to the conventional case, as shown in Fig. 8.

Fig. 9(a) shows the velocity profiles along the radial direction at the expansion pipe inlet (or outlet of pipe nozzle), and Fig. 9(b) shows the pressure profiles on impingement surface of the central jet. The peaks of velocity profiles at *r*/*d* = 0.5 were for the jet flow region, and the profiles in the range of 0.5 < *r*/*d* < 2.0 were for the section where surrounding air enters into the expansion pipe. The velocity profiles in the air-entrained section were higher for the longer expansion pipe length. Longer expansion pipe length evidently induces surrounding air into the expansion pipe due to the low pressure created inside the pipe, and hence a greater suction force. This influences directly on jet momentum impinging on the target surface, which could be identified by getting higher pressure

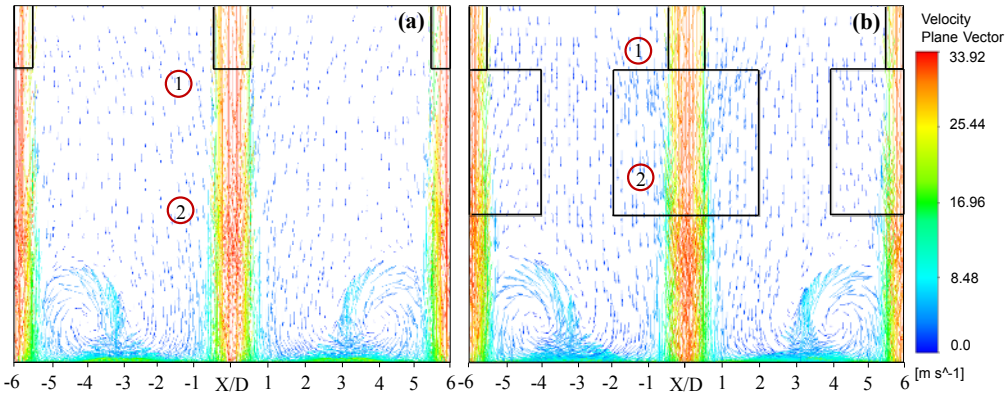

Fig. 7. Velocity-vector field of impinging jets on *Z-X* plane at the center of nozzle: (a) Conventional jets; (b) jets with expansion pipes at L/d = 4 and S/d = 6 at fixed H/d = 8, (CFD results, Re = 30000).

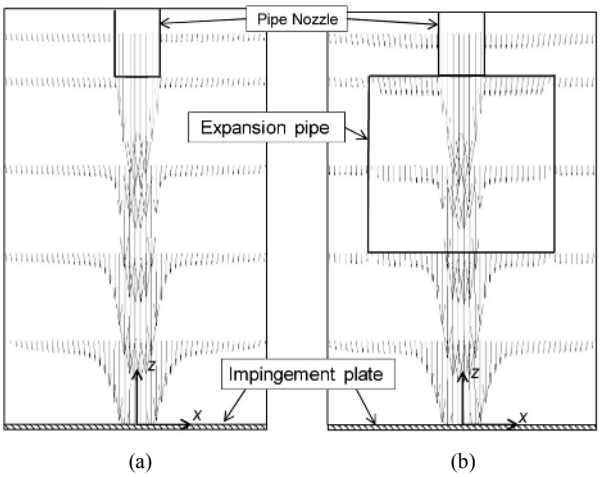

Fig. 8. Velocity-vector field of impinging jet on *Z-X* plane at middle nozzle on Y/d = 0: (a) Conventional jets; (b) jet with expansion pipes at L/d = 4 and S/d = 6 at fixed H/d = 8 (CFD results, Re = 30000).

distributions of longer expansion pipe length as shown in Fig. 9(b).

In short, this study has demonstrated that mounting of an expansion pipe at the jet outlet can induce the surrounding air into the jet flow. When the expansion pipe is longer, moreover, the surrounding air entering into the expansion pipe is greater. Effects on heat transfer on the impingement surface involving the use of such mounting with various lengths are discussed next in Sec. 4.2.

4.2 Heat transfer characteristics

Fig. 10 illustrates Nusselt number contours on the impingement surface. A small circle mark indicates the location of the pipe nozzle, and a large the expansion pipe. Nusselt number distribution on the surface is categorized into two regions: an area of high Nusselt number ($Nu \geq 90$) indicating stagnation region where a jet impinges directly, and an area of low Nusselt number ($Nu < 90$), indicating a jet interval region where spent jets accumulate and vent out.

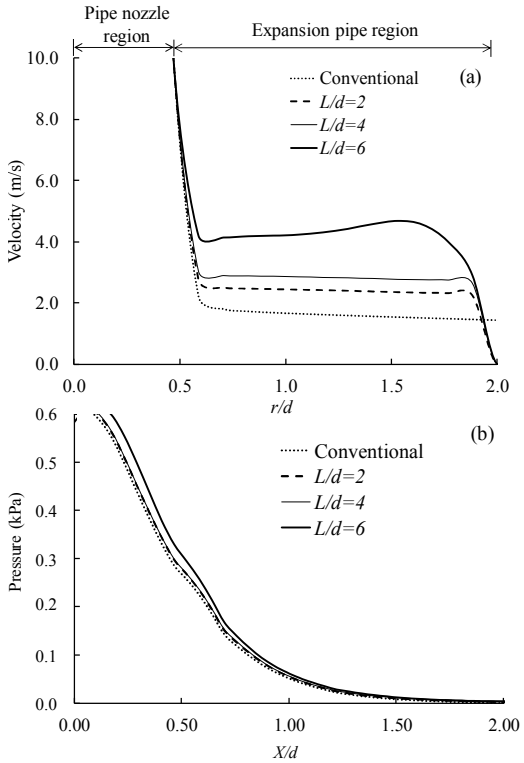

Fig. 9. (a) Velocity profile of jet and surrounding air on *Z-X* plane at middle nozzle outlet on $0 \leq r/d \leq 2$; (b) pressure profile on impingement surface of central jet (CFD results, S/d = 6, H/d = 8, Re = 30000).

The figure is shown in four sets: one employing conventional jet having S/d of 6 and 8, and three other sets employing jet with expansion pipe having L/d of 2, 4 and 6. Nusselt number distributions in the stagnation region for jets with expansion pipe were markedly higher than those in the case of conventional jets, especially at the center of jet impingement. This is a direct effect of mounting the expansion pipe at the nozzle outlet, which accelerates the surrounding air entering into the expansion pipe and mixing with the jet flow as discussed regarding flow characteristics in Sec. 4.1. This could

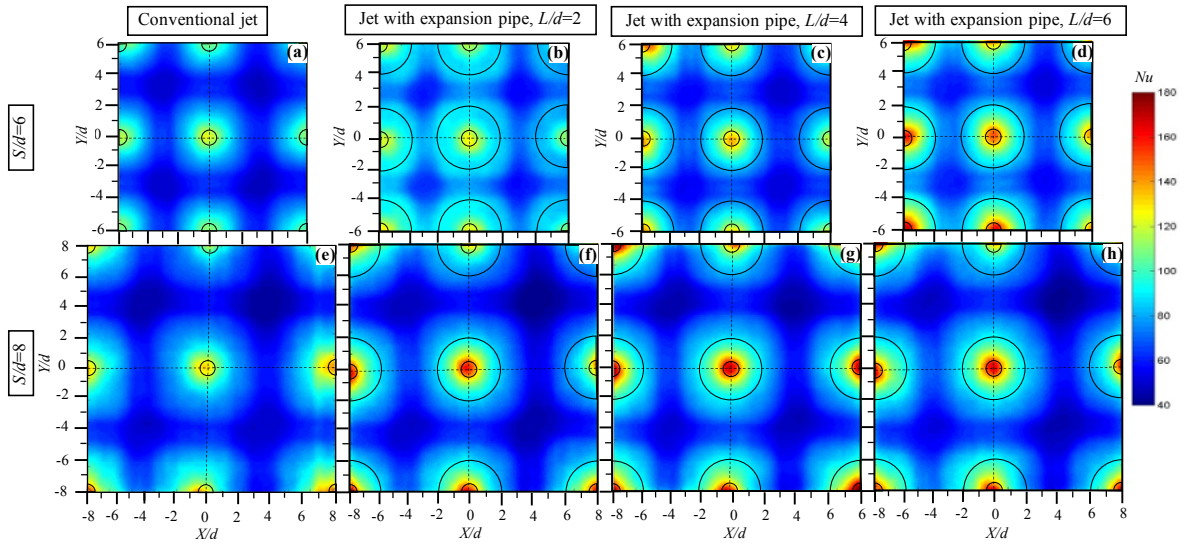

Fig. 10. Nusselt number contours on the impingement surface at fixed H/d = 8, Re = 30000 (experimental results).

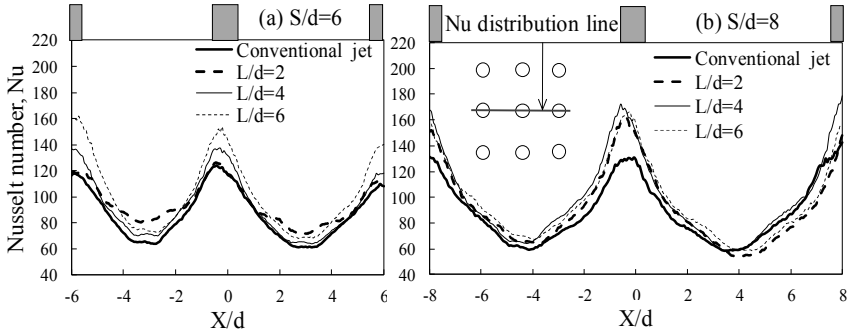

Fig. 11. Nusselt number distributions on the impingement surface along nozzle centerline (Y/d = 0): (a) S/d = 6; (b) S/d = 8 (experimental results, Re = 30000, rectangular symbols indicating nozzle locations).

be justified by getting high pressure distributions due to high jet momentum impinging on the surface for the case of mounting expansion pipe as previously shown in Fig. 9(b).

At jet-to-jet spacing S/d = 6 for jets with expansion pipe (Figs. 10(b)-(d)), the Nusselt number at the stagnation point became increasingly higher when the expansion pipe length got longer, while at S/d = 8 (Figs. 10(f)-(h)), the Nusselt number was not much affected by the expansion pipe length. In all cases, however, Nusselt numbers at stagnation point for the expansion pipe setting were higher than that without the expansion pipe.

For the jet interval region, it appears that the mounting expansion pipe could only enhance Nusselt number in the case of S/d = 6 (Figs. 10(b)-(d)), as compared with that using conventional jets (Fig. 10(a)). At the larger jet-to-jet spacing S/d = 8 (Figs. 10(f)-(h)), the Nusselt numbers were quite comparable to that in the conventional setting (Fig. 10(e)). Thus, it could be safely deduced that for a larger jet spacing, the expansion pipe length has a smaller and smaller effect.

Referring back to S/d = 6, the 'area' of high Nusselt number (Nu > 90) at stagnation region for the case of jet with expansion pipe at L/d = 2 (Fig. 10(b)) is notably higher than the case of L/d = 4 and 6 (Figs. 10(c) and (d)). This is from the effect of jet-to-jet interaction before impingement in the case of short expansion pipe length and narrow jet-to-jet spacing. For the longer expansion pipe length, the surrounding air entering into the expansion pipe was high, but jet-to-jet interaction was low due to blocking of the longer pipe.

In Fig. 11, Nusselt number distributions along X/d direction at the nozzle centerline (Y/d = 0) are shown, and in Fig. 12, at the jet intervals (Y/d = 3 for S/d = 6 and Y/d = 4 for S/d = 8). The rectangular symbols at the top of both figures indicate the nozzle locations. According to Fig. 11(a) for S/d = 6, the peak of the Nusselt number at the stagnation point for the case of expansion pipe became higher when the pipe was longer, agreeing with the result from surrounding air entering into the expansion pipe that the velocity profile was higher when the expansion pipe length was longer. This could be explained as that the induced air increases jet mixing, resulting in increasing turbulent intensity of the jets and increasing jet momentum impinging on the target surface (as shown high pressure distribution in Fig. 9(b)). Longer expansion pipe length thus certainly increases heat transfer at stagnation point for S/d = 6. Nevertheless, for other areas on the impingement surface, heat

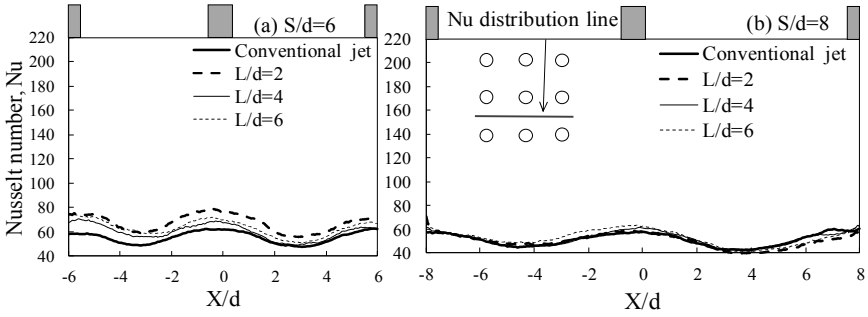

Fig. 12. Nusselt number distributions on the impingement surface along nozzle interval: (a) S/d = 6 at Y/d = 3; (b) S/d = 8 at Y/d = 4 (experimental results, Re = 30000, rectangular symbols indicating nozzle location.

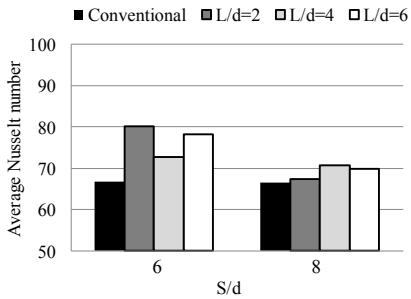

Fig. 13. Comparison of average Nusselt number on the impingement surface (experimental results, Re = 30000).

transfer enhancement appeared to be not a function of the length of expansion pipe, as evidenced at the troughs in the Figure.

For the larger S/d = 8 in Fig. 11(b), the peaks of Nusselt number at stagnation point of jets with expansion pipe for all L/d cases were more or less comparable; however, all peaks were higher than the case of conventional jets. This implies that the expansion pipe length has no significant effect in the case of large jet-to-jet spacing, but the expansion pipe did surely influence the increase of heat transfer for every L/d cases when compared with the without-expansion pipe setting.

Fig. 12 shows cross-sections along a jet interval. At S/d = 6, the Nusselt number distributions for the case of expansion pipe were significantly higher than that of conventional jets, whereas at S/d = 8, the results were approximately the same whether with a mounting expansion pipe, or not. Thus a larger spacing would yield a less desirable outcome.

4.3 Average Nusselt number

The average Nusselt numbers calculated from the average temperature using Eq. (4) over a 3 rows × 3 columns middle area of jets are shown in Fig. 13. Generally, values for the case of jets with expansion pipe are higher than for conventional jets. Nusselt number enhancement employing the mounting expansion pipe in the case of the narrower jet-to-jet spacing (S/d = 6) was found to be more influential than that of the wider jet-to-jet spacing (S/d = 8). The average value tends to increase with longer expansion pipe; however, an exception occurred in the case of S/d = 6 and L/d = 2 in that its average

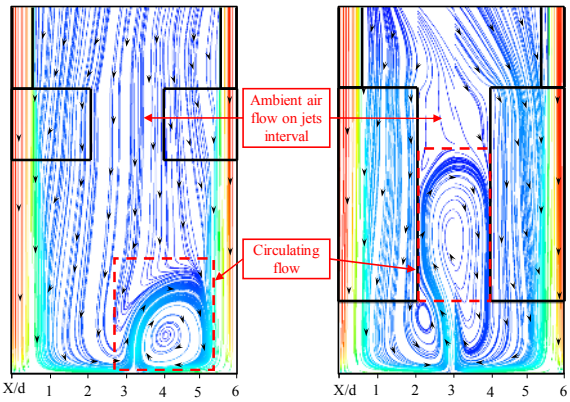

Fig. 14. Streamline of velocity for middle and adjacent jet on Z-X plane at 0≤X/d≤6, S/d = 6 at fixed H/d = 8: (a) Jets with expansion pipes at L/d = 2; (b) jets with expansion pipes at L/d = 6 (CFD results, Re = 30000).

Nusselt number was outstandingly higher than all other cases.

As it turned out, the expansion pipe length affected jet flows, as can be visualized from CFD streamlines in Fig. 14. For the shortest pipe (L/d = 2), the wall jets in the jet interval region were mixed with jet flows after impingement and enhanced high heat transfer on the surface. For the longest pipe (L/d = 6), the wall jets in the jet interval region developed large circulation flows that blocked the surrounding air entering to mix with the jet flow. Thus, it is clear that a longer expansion pipe length could yield a better heat transfer, up to a limit due to blocking of air circulation, and that an appropriate shorter one could render a superior result.

As a result, the average Nusselt number of the jets with mounting expansion pipe for S/d = 6 was highest at L/d = 2, and hence most efficient on heat transfer. This represents a 19.82 % increase to the case of the use of conventional jets. For S/d = 8, the average Nusselt number of the jets with expansion pipe was highest at L/d = 4, rendering a 6.27 % higher efficiency than the case without an expansion pipe.

5. Conclusions

Effects of expansion pipe length on heat transfer enhancement and flow characteristics have been experimentally and

numerically investigated in this study. Main results can be summarized as follows:

(1) Mounting expansion pipe induces surrounding air into the jet flow and hence better heat transfer efficiency than the use of conventional jets without one, up to nearly 20 % in this research.

(2) Enhancement of heat transfer at the point normal to the jet flow, or the stagnation point, was found to be better for a narrower jet-to-jet spacing (S/d = 6 vs. S/d = 8). This should be further investigated for an even better spacing of jet nozzles with mounted expansion pipes.

(3) Though surrounding air entering into the expansion pipe is greater when the expansion pipe is longer, this does not necessarily always lead to a better heat transfer efficiency due to blocking of flow circulation when the expansion pipe gets too long. The average heat transfer on the impingement surface for the case of jets with mounting expansion pipe at the pipe length of L/d = 2, and not at L/d = 4 or L/d = 6, and narrow jet-to-jet spacing S/d = 6 was found to be the highest due to accumulation of larger area of high heat transfer in jet interval regions.

Acknowledgments

This study was supported by the Thailand Research Fund (Grant No. MGR5980082). We also thank Mr. Wiwat Sutiwipakorn, department of civil engineering, Prince of Songkla University, for editing the manuscript.

Nomenclature

A : Stainless steel foil area (mm)
d : Nozzle inner diameter (mm)
D : Expansion pipe inner diameter (mm)
L : Expansion pipe length (mm)
H : Jet-to-wall distance (mm)
h : Local heat transfer coefficient (W/m^2·K)
$h_{loss,c}$: Natural convective heat transfer coefficient (W/m^2·K)
$\overline{h}$: Average heat transfer coefficient (W/m^2·K)
I : Electrical current (A)
k : Thermal conductivity of jet (W/m·K)
Nu : Nusselt number (-)
$\overline{Nu}$: Average Nusselt number (-)
$\dot{Q}_{input}$: Input heat flux (W/m^2)
$\dot{Q}_{loss,c}$: Heat loss from convection (W/m^2)
$\dot{Q}_{loss,r}$: Heat loss from radiation (W/m^2)
Re : Reynolds number (-)
S : Jet-to-jet spacing (mm)
T_{aw} : Adiabatic wall temperature (°C)
T_w : Wall temperature (°C)
T_s : Surround temperature (°C)
u_τ : Friction velocity (m/s)
V : Voltage (V)
v : Kinematic viscosity of air (m^2/s)
y^+ : Dimensionless wall distance (-)
y_1 : Distance of the first node to the wall (mm)

Greek symbols

σ : Stefan-Boltzmann constant (W/m^2·K^4)
ε : Emissive coefficient (-)

References

[1] K. Jambunathan et al., A review of heat transfer data for single circular jet impingement, *International J. of Heat and Fluid Flow,* 13 (2) (1992) 106-115.

[2] R. Viskanta, Heat transfer to impinging isothermal gas and flame jets, *Experimental Thermal and Fluid Science,* 6 (2) (1993) 111-134.

[3] H. Martin, Heat and mass transfer between impinging gas jets and solid surfaces, *Advances in Heat Transfer*, 13 (1977) 1-60.

[4] B. R. Hollworth and R. D. Berry, Heat transfer from arrays of impinging jets with large jet-to-jet spacing, *J. of Heat Transfer*, 100 (2) (1978) 352-357.

[5] A. M. Huber and R. Viskanta, Effect of jet-jet spacing on convective heat transfer to confined, impinging arrays of axisymmetric air jets, *International J. of Heat and Mass Transfer,* 37 (18) (1994) 2859-2869.

[6] L. F. G. Geers, M. J. Tummers, T. J. Bueninck and K. Hanjalic, Heat transfer correlation for hexagonal and in-line arrays of impinging jets, *International J. of Heat and Mass Transfer*, 51 (21-22) (2008) 5389-5399.

[7] N. Gao, H. Sun and D. Ewing, Heat transfer to impinging round jets with triangular tabs, *International J. of Heat and Mass Transfer*, 46 (14) (2003) 2557-2569.

[8] S. J. Lee, Y. G. Jang and Y. S. Choi, Stereoscopic-PIV measurement of turbulent jets issuing from a sharp-edged circular nozzle with multiple triangular tabs, *J. of Mechanical Science and Technology,* 26 (9) (2012) 2765-2771.

[9] G. Cafiero, G. Castrillo, C. S. Greco and T. Astarita, Effect of the grid geometry on the convective heat transfer of impinging jets, *International J. of Heat and Mass Transfer*, 104 (2017) 39-50.

[10] P. Muvvala, C. Balaji and S. P. Venkateshan, Experimental investigation on the effect of wire mesh at the nozzle exit on heat transfer from impinging square jets, *Experimental Thermal and Fluid Science,* 84 (2017) 78-89.

[11] S. Eiamsa-ard and W. Changcharoen, Flow structure and heat transfer in a square duct fitted with dual/quadruple twisted-tapes: Influence of tape configuration, *J. of Mechanical Science and Technology,* 29 (8) (2015) 3501-3518.

[12] A. Saysroy, W. Changcharoen and S. Eiamsa-ard, Performance assessment of turbular heat exchanger tubes containing rectangular-cut twisted tapes with alternate axes, *J. of Mechanical Science and Technology,* 32 (1) (2018) 433-445.

[13] C. Nuntadusit, M. Wae-hayee, A. Buyajitradulya and S. Eiamsa-ard, Heat transfer enhancement by multiple swirling impinging jets with twisted-tape swirl generators, *International Communications in Heat and Mass Transfer*, 39 (1) (2012) 102-107.

[14] C. Nuntadusit, M. Wae-hayee, A. Bunyajitradulya and S. Eiamsa-ard, Visualization of flow and heat transfer characteristics for swirling impinging jet, *International Communications in Heat and Mass Transfer,* 39 (5) (2012) 640-648.

[15] S. V. Alekseenko, A. V. Bilsky, V. M. Dulin and D. M. Markovich, Experimental study of an impinging jet with different swirl rates, *International J. of Heat and Fluid Flow,* 28 (6) (2007) 1340-1359.

[16] M. Fenot, E. Dorignac and G. Lalizel, Heat transfer and flow structure of a multichannel impinging jet, *International J. of Thermal Sciences*, 90 (2015) 323-338.

[17] X. T. Trinh, M. Fenot and E. Dorignac, The effect of nozzle geometry on local convective heat transfer to unconfined impinging air jets, *Experimental Thermal and Fluid Science,* 70 (2016) 1-16.

[18] R. Vinze, S. Chandel, M. D. Limaye and S. V. Prabhu, Local heat transfer distribution between smooth flat surface and impinging incompressible air jets from a chevron nozzle, *Experimental Thermal and Fluid Science,* 78 (2016) 124-136.

[19] W. C. Selerowicz, A. P. Szumowski and G. E. A. Meier, Self-excited compressible flow in a pipe-collar nozzle, *J. of Fluid Mechanics,* 228 (1991) 465–485.

[20] Y. Zeng, T. H. New and T. L. Chng, Flow behavior of turbulent nozzle jets issuing from bevelled collars, *Experimental Thermal and Fluid Science,* 35 (8) (2011) 1555-1564.

[21] G. J. Nathan, J. Mi, Z. T. Alwahabi, G. J. R. Newbold and D. S. Nobes, Impacts of a jet's exit flow pattern on mixing and combustion performance, *Progress in Energy and Combustion Science*, 32 (5-6) (2006) 496-538.

[22] K. Yeranee, M. Wae-hayee, I. Piya, Y. Rao and C. Nuntadusit, The study of flow and heat transfer characteristics of impinging jet array mounting air-induced duct, *IOP Conference Series: Materials Science and Engineering*, 243 (2017).

[23] C. Nuntadusit, M. Wae-hayee and N. Kaewchoothong, Heat transfer enhancement on a surface of impinging jet by increasing entrainment using air-augmented duct*, International J. of Heat and Mass Transfer*, 127 (2018) 751-767.

[24] S. Kline and F. Mcclintock, Describing uncertainties in single-sample experiments, *Mechanical Engineering*, 75 (1953) 3-8.

[25] P. Gulati, V. Katti and S. V. Prabu, Influence of the shape of the nozzle on local heat transfer distribution between smooth flat surface and impinging air jet, *International J. of Thermal Sciences,* 48 (3) (2009) 602-617.

[26] V. Katti and S. V. Prabhu, Experimental study and theoretical analysis of local heat transfer distribution between smooth flat surface and impinging air jet from a circular straight pipe nozzle, *International J. of Heat and Mass Transfer,* 51 (17-18) (2008) 4480-4495.

[27] Q. Y. Zhao, H. Chung, S. M. Choi and H. H. Cho, Effect of guide wall on jet impingement cooling in blade leading edge channel, *J. of Mechanical Science and Technology*, 30 (2) (2016) 525-531.

[28] N. Zuckerman and N. Lior, Jet impingement heat transfer: physics, correlations and numerical modeling, *Advances in Heat Transfer*, 39 (2006) 565-631.

[29] M. Behnia, S. Parneix and P. A. Durbin, Prediction of heat transfer in an axisymmetric turbulent jet impinging on a flat plate, *International J. of Heat and Mass Transfer,* 41 (12) (1998) 1845-1855.

[30] B. Sunden, J. Larocque and Z. Wu, Numerical simulation of heat transfer from impinging swirling jets, *Impingement Cooling in Gas Turbines: Design, Applications, and Limitations* (2014) 185-203.

[31] M. Wae-hayee, P. Tekasakul, S. Eiamsa-ard and C. Nuntadusit, Effect of cross-flow velocity on flow and heat transfer characteristics of impinging jets with low jet-to-plate distance, *J. of Mechanical Science and Technology*, 28 (7) (2014) 2909-2917.

[32] M. Ghorbani, M. Yildiz, D. Gozuacik and A. Kosar, Cavitating nozzle flows in micro- and minichannels under the effect of turbulence, *J. of Mechanical Science and Technology*, 30 (6) (2016) 2565-2581.

Kirttayoth Yeranee is currently a Master's student in international double degree program in the Department of Mechanical Engineering, Prince of Songkla University (PSU), Thailand and School of Mechanical Engineering, Shanghai Jiao Tong University (SJTU), China. His interests include impinging jet, heat transfer enhancement and CFD.

Makatar Wae-hayee is a lecturer in the Department of Mechanical Engineering, Prince of Songkla University (PSU), Thailand. He received Ph.D. at the same university in 2014. His interests concern flow and heat transfer, CFD and thermal-fluid engineering.

Ibroheng Piya is lecturer in the Department of Mechanical Engineering, Princess of Naradhiwas University (PNU), Thailand. He received the Master's in Engineering in Mechanical Engineering from Prince of Songkla University (PSU), Thailand in 2013. His research interest includes flow and heat transfer engineering.

Yu Rao is a Professor at Institute of Turbomachinery, School of Mechanical Engineering, Shanghai Jiao Tong University, China. He received the Ph.D. in Aeronautics and Astronautics at Beijing University, and TU Darmstadt in Germany in 2006. His current interests include gas turbine aerodynamics, heat transfer and cooling technology.

Chayut Nuntadusit is an Assistant Professor of Mechanical Engineering at Prince of Songkla University, Thailand. He received the Ph.D. at Osaka University in 2004. His current interests include heat transfer enhancement for jet impingement, jet flow control and optical measurement.